arXiv:1612.07327v1 [cond-mat.stat-mech] 21 Dec 2016

Operator entanglement entropy of the time evolution operator in chaotic systems

Tianci Zhou[1] and David J. Luitz[1]

[1] *Institute for Condensed Matter Theory and Department of Physics, University of Illinois at Urbana-Champaign, Urbana, IL 61801, USA*[*]

(Dated: December 23, 2016)

We study the growth of the operator entanglement entropy (EE) of the time evolution operator in chaotic, many-body localized and Floquet systems. In the random field Heisenberg model we find a universal power law growth of the operator EE at weak disorder, a logarithmic growth at strong disorder, and extensive saturation values in both cases. In a Floquet spin model, the saturation value after an initial linear growth is identical to the value of a random unitary operator (the Page value). We understand these properties by mapping the operator EE to a global quench problem evolved with a similar parent-Hamiltonian in an enlarged Hilbert space with the same chaotic, MBL and Floquet properties as the original Hamiltonian. The scaling and saturation properties reflect the spreading of the state EE of the corresponding time evolution. We conclude that the EE of the evolution operator should characterize the propagation of information in these systems.

PACS numbers: 03.67.Bg,05.45.Mt,75.10.Pq

I. INTRODUCTION

Chaotic behavior is usually associated with a rapid loss of information about the initial state of a system. In quantum systems, this can for example be quantified by studying the time dependence of measures for quantum information, most notably for the entanglement of two subsystems. Typically, chaotic systems will quickly entangle the susbsystems over time, even if they are initially in a product state and the spread of entanglement is usually faster than the transport of particles.

The dynamical process of thermalization can be studied by a quench, where the initial state is prepared for example as the groundstate of a local Hamiltonian H_0 and the Hamiltonian is suddenly changed to another Hamiltonian H of interest, governing the time evolution of the wave function. Thermalization can then be monitored by various quantities, among which the entanglement entropy (EE) provides a particularly appealing measure, since it encodes the scrambling of information about the initial state. In generic quantum systems, it grows very fast (a power law[1], except for the logarithmic growth in MBL systems[1–5]) until it saturates to a large value which scales as the volume of the system and is determined by the initial state (which itself is usually constructed to have low entanglement).

While this scenario is very well studied, it seems clear that the scrambling of information about the initial state is not a property of the wave function, but rather that of the Hamiltonian. This is particularly plausible when thinking of two extreme cases, a generic system with diffusive transport, which exhibits a ballistic growth of the quench EE[1,6], compared to an MBL system, where the growth of the quench EE is logarithmic in time and thus very slow, *while using the same initial product state in both cases*. A multitude of previous works has established the differences of these two classes of systems regarding aspects of the eigenvalues and eigenvectors of the Hamiltonian, exhibiting *e.g.* volume- vs area-law entanglement entropy[7–13] and the validity or violation[12,14,15] of the eigenstate thermalization hypothesis[16–18], all revealing properites of the Hamiltonian.

Motivated by the success of the study of the quench EE, we propose here to study the operator entanglement entropy (opEE)[19–21] of the *time evolution operator*, which is probably simplest to be described in the matrix product operator (MPO) language[22]. As shown in Fig. 1, an operator can be viewed as a matrix product state with two copies of physical indices. Then its entanglement entropy can be similarly defined as for the state. Since the time evolution operator of a local Hamiltonian

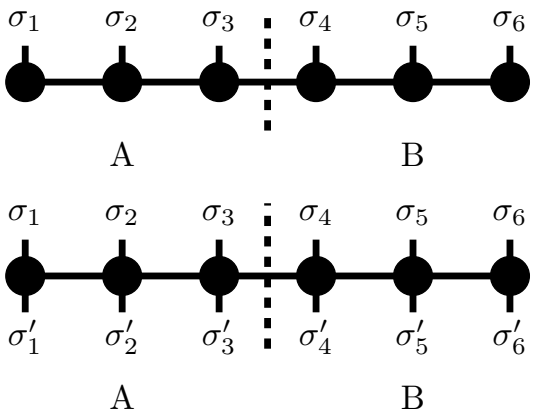


FIG. 1. Matrix product state (MPS) and matrix product operator (MPO). Upper panel: diagrammatic representation of matrix product state. Each tip of the vertical bond is a physical index; horizontal bonds contract auxillary matrix indices. After performing a left and right canonicalization up to one bond, the chosen bond will contain all the Schmidt eigenvalues that determine the entanglement entropy. Bottom panel: the matrix product operator can be viewed as a matrix product state with two copies of physical indices on each site, then its entanglement entropy can be similarly defined and calculated by a matrix product algorithm.

clearly contains all the information for all possible initial states and correlates distant parts of the system increasingly with time, we expect that its opEE will grow with time and possibly saturate close to its maximal value.

We note that the operator entanglement entropy is the relevant quantity for the efficiency of encoding operators as an MPO[3,20], since it governs the required bond dimension. In the context of MBL, it was shown that the Hamiltonian is diagonalized by a unitary operator that can be represented by an MPO with finite bond dimension and therefore low opEE[23,24], compared to the case of a chaotic system, where we expect the opEE of the diagonalizing operator to be a volume law.

In this paper, we present the concept of the opEE of the time evolution operator and demonstrate that it grows as a power law in time for generic quantum systems up to a saturation value which scales as the volume of the system. In Sec. II, we define the opEE of time evolution operator. In Sec. III, we map the opEE to the state EE in a quench problem as a way to understand the general growth and saturation behaviors. Then in Sec. IV we introduce the spin chain models and discuss in detail the growth and saturation of their opEE in Sec. VI and V. Finally we conclude in Sec. VII. App. A introduces the channel-state duality to understand opEE. App. B contains a technical calculation of average opEE of random unitary operators. App. C contains the numerical technique we used for a conserved sector of the Heisenberg spin chain.

II. OPERATOR ENTANGLEMENT ENTROPY (OPEE) OF THE TIME EVOLUTION OPERATOR

A. Definition

We begin by reviewing the definition of entanglement entropy for a pure state. Then by assigning a Hilbert space structure for linear operators, we show that the time evolution operator is a normalized "wave function" in the operator space and therefore the entanglement entropy for it can be naturally defined.

1. *Wave function entanglement entropy*

For a real space bipartition into subsystems A and B, a pure state $|\psi\rangle$ in the Hilbert space $\mathcal{H}$ can be represented in a basis which is the tensor product of the orthonormal bases of the two subsystems $\{|i\rangle_A\}$ and $\{|j\rangle_B\}$:

$$|\psi\rangle = \sum_{ij} \psi_{ij} |i\rangle_A \otimes |j\rangle_B \tag{1}$$

where the coefficients are given by the inner product

$$\psi_{ij} = \left({}_A\langle i| \otimes {}_B\langle j|\right) |\psi\rangle. \tag{2}$$

The reduced density matrix of subsystem A is then obtained by performing the partial trace of the pure density matrix $|\psi\rangle\langle\psi|$ over the subsystem B:

$$\rho_A = \mathrm{Tr}_B |\psi\rangle\langle\psi| \quad \Rightarrow \quad \rho^A_{ij} = \sum_k \psi_{ik}\psi^*_{jk} \tag{3}$$

and the von Neumann entanglement entropy (which corresponds to the Rényi entropy with Rényi index $q = 1$) is the Shannon entropy of its eigenvalues λ_n:

$$S_A = -\mathrm{Tr}(\rho_A \ln \rho_A) = -\sum_n \lambda_n \ln \lambda_n. \tag{4}$$

2. *Operator entanglement entropy*

The concept of the entanglement entropy introduced above has been generalized to the space of operators[19], which is also a Hilbert space $\{\mathfrak{O}, (\cdot,\cdot)\}$ with the inner product $(\cdot,\cdot) : \mathfrak{O}\times\mathfrak{O} \to \mathbb{C}$ on the space of linear operators $\mathfrak{O}$ on $\mathcal{H}$. The inner product for two operators $\hat{O}_1, \hat{O}_2 \in \mathfrak{O}$ is defined by

$$(\hat{O}_1, \hat{O}_2) = \frac{1}{\sqrt{\dim(\mathfrak{O})}} \mathrm{Tr}(\hat{O}_1^\dagger \hat{O}_2). \tag{5}$$

Here $\dim(\mathfrak{O}) = \dim(\mathcal{H})^2$ is the dimension of the operator space. We can now construct two complete basis sets $\{\hat{A}_i\}$ and $\{\hat{B}_i\}$ which are orthonormal with respect to the inner product (5) and consist only of operators with a support on the subsystems A and B respectively. The two bases span operator spaces $\mathfrak{O}_A = \mathrm{span}(\{\hat{A}_i\})$ on the subsystem A (and B respectively) and their tensor product is the full operator space $\mathfrak{O} = \mathfrak{O}_A \otimes \mathfrak{O}_B$.

For any linear operator $\hat{O} \in \mathfrak{O}$, we then have a unique decomposition

$$\hat{O} = \sum_{ij} O_{ij} \hat{A}_i \otimes \hat{B}_j \tag{6}$$

with coefficients $O_{ij} \in \mathbb{C}$ obtained by the inner product

$$O_{ij} = (\hat{A}_i \otimes \hat{B}_j, \hat{O}). \tag{7}$$

In particular, we consider the unitary evolution operator

$$\hat{U}(t) = \mathcal{T} e^{-i\int_0^t H(t')dt'} \tag{8}$$

given in general by a time ordered exponential. It propagates the wave function from time zero to time t and satisfies the unitary condition at all times t

$$\left(\hat{U}(t), \hat{U}(t)\right) = \frac{1}{\dim(\mathcal{H})} \mathrm{Tr}\left[\hat{U}(t)^\dagger \hat{U}(t)\right] = 1. \tag{9}$$

As a result, it is a normalized element of the operator space $\mathfrak{O}$ in the same way as a normalized wave function in the Hilbert space $\mathcal{H}$.

With these ingredients, we can define the *operator entanglement entropy* (opEE) as the Shannon entropy of the eigenvalues of the reduced *operator density matrix*

$$S = -\mathrm{Tr}(\rho_{\mathrm{op}}^A \ln \rho_{\mathrm{op}}^A) \tag{10}$$

where the operator reduced density matrix in this basis is

$$(\rho_{\mathrm{op}}^A)_{ij} = \sum_k U_{ik}(U^\dagger)_{kj}, \tag{11}$$

with $U_{ij} = (\hat{A}_i \otimes \hat{B}_j, \hat{U}(t))$.

When $t = 0$, the evolution operator is the identity operator and hence has zero initial opEE. As t increases, the operator becomes more and more complicated and we expect the opEE to reflect the complexity of the time evolution. To ease the notation, we will drop the hat if its operator nature is clear in the context, but will reserve it in figures to make the difference to the usual "state" EE explicit.

III. GENERAL BEHAVIOR OF OPEE

A. Mapping to Quench

It is useful to map the opEE of the time evolution operator to a quench problem in a larger Hilbert space, since this allows us to connect to known features of the wave function entanglement entropy. In App. A, we introduce one possible mapping via the channel-state duality, but this is not the only possibility(see[19] for another map in Majorana representation). Let us introduce below a different mapping preserving locality, which makes it easier to identify the general features of the opEE of the time evolution operator as a function of time in finite systems. Specifically, for an evolution operator (of a time independent Hamiltonian) $U(t) = e^{-iHt}$, our goal is to construct a corresponding $\overline{H}$ and state $|\psi\rangle$, such that state EE of $e^{-i\overline{H}t}|\psi\rangle$ is the same as opEE of $U(t)$ under the same real space partition:

$$U(t) = e^{-iHt} \quad \leftrightarrow \quad e^{-i\overline{H}t}|\psi\rangle. \tag{12}$$

We will see in the next two subsections that in the MBL phase, a simple choice is

$$\overline{H} = H, \quad |\psi\rangle = \otimes_{i=1}^L |\uparrow\rangle \tag{13}$$

where L is the number of sites. Whereas for a generic Hamiltonian, $|\psi\rangle$ can be taken as

$$|\psi\rangle = \otimes_{i=1}^{2L} |\uparrow\rangle \tag{14}$$

which is in a two-copy Hilbert space $\mathcal{H} \otimes \mathcal{H}$ that can represent all possible operators in $\mathfrak{O}$. $\overline{H}$ in this case will be an operator acting on $\mathcal{H} \otimes \mathcal{H}$, which we will construct explicitly below.

1. MBL Hamiltonian

In the MBL phase the Hamiltonian is effectively given by multi-spin interaction terms between the "l-bits" σ_i^x[5,25–30]

$$H_{\mathrm{MBL}} = \sum_i h_0^i \sigma_i^x + \sum_{ij} J_{ij}^0 \sigma_i^x \sigma_j^x + \sum_{ijk} J_{ijk}^0 \sigma_i^x \sigma_j^x \sigma_k^x + \cdots \tag{15}$$

The "l-bits" are local integrals of motion, and the exponentially (with distance) decaying interactions between them are responsible for the slow entanglement dynamics in MBL systems[1–5,31]. For this particular type of Hamiltonian, the time evolution operator $U(t)$ will only consist of products of the identity operator $I \equiv \sigma^0$ and σ^x. In contrast, the local basis of the complete operator space $\mathfrak{O}$ consists of the 4 elements I_i, σ_i^x, σ_i^y and σ_i^z on site i of the system. This means that the MBL time evolution operator is only contained in a subspace of dimension 2^L of the total operator Hilbert space $\mathfrak{O}$ which has the dimension $\dim(\mathfrak{O}) = 4^L$. This allows us to map the evolution operator to a state Hilbert space of dimension 2^L *without doubling the number of degrees of freedom.*

Note that the states $|\uparrow\rangle = I|\uparrow\rangle$ and $|\downarrow\rangle = \sigma^x|\uparrow\rangle$ are orthonormal in the single-site Hilbert space and we can therefore map $I \to I|\uparrow\rangle$ and $\sigma^x \to \sigma^x|\downarrow\rangle$. In the multiple-site situation, the basis which only consists of products of $I \equiv \sigma^0$ and σ^x

$$\sigma_1^{\mu_1}\sigma_1^{\mu_2}\cdots\sigma_L^{\mu_L} \quad \mu_i = 0 \text{ or } 1 \tag{16}$$

can be mapped to orthonormal basis in $\mathcal{H}$ as

$$\sigma_1^{\mu_1}\sigma_1^{\mu_2}\cdots\sigma_L^{\mu_L}|\uparrow\cdots\uparrow\rangle. \tag{17}$$

Then the decomposition of $U(t)|\uparrow\ldots\uparrow\rangle$ in the state basis is identical to the decomposition of $U(t)$ in the operator basis and the state EE of the wave function after a global quench from the state $|\uparrow\cdots\uparrow\rangle$ given by $|\psi(t)\rangle = U(t)|\uparrow\cdots\uparrow\rangle$ is identical to the opEE. Therefore in this case the bar transformation is the trivial identity map and $|\psi\rangle = \otimes_{i=1}^L|\uparrow\rangle$.

Applying well known results on the logarithmic EE growth after a quench from a product state in MBL systems[1–5,31], this mapping immediately implies a logarithmic long time growth and an extensive submaximal saturation value of the opEE in MBL systems and therefore gives an initial state independent description of the information propagation in MBL.

2. Generic Hamiltonian

A completely generic (and possibly non-local) Hamiltonian can be composed of all possible spin interactions

$$H = \sum_{\mu_1,\mu_2,\cdots,\mu_L=0}^{3} J_{\mu_1\mu_2\cdots\mu_L}\sigma_1^{\mu_1}\sigma_2^{\mu_1}\cdots\sigma_L^{\mu_1}, \tag{18}$$

where $\sigma^0 \equiv I$ is understood as identity operator and $J_{\mu_1\mu_2\cdots\mu_L}$ are complex interaction coefficients (this is in fact an operator basis decomposition of the Hamiltonian). It occupies the full operator Hilbert space $\mathfrak{O}$, and so by dimensional counting, it is only possible to map the operator to a double-site state Hilbert space $\mathcal{H}\times\mathcal{H}$. In order to do so, we equip each site with an auxiliary site and upgrade the Hamiltonian H to

$$\overline{H} = \sum_{\mu_1,\mu_2,\cdots,\mu_L=0}^{3} J_{\mu_1\mu_2\cdots\mu_L}\overline{\sigma}_1^{\mu_1}\overline{\sigma}_2^{\mu_1}\cdots\overline{\sigma}_L^{\mu_1}, \tag{19}$$

where each $\overline{\sigma}$ is acting on both the physical site and the nearby auxiliary site. For one dimensional systems, it is helpful to think of the new Hamiltonian $\overline{H}$ as a ladder system (bilayer for 2d), which implies that the locality features of the initial system are preserved. The "bar" transformation is defined by the mapping

$$\begin{aligned} \overline{I} &= I\otimes I, \qquad \overline{\sigma}^x = \sigma^x\otimes\sigma^x, \\ \overline{\sigma}^y &= \sigma^y\otimes\sigma^x, \quad \overline{\sigma}^z = \sigma^z\otimes\sigma^x, \end{aligned} \tag{20}$$

where we introduce a σ^x operator on auxiliary degrees of freedom for every operator except for the identity (producing an identity on the auxiliary site).

The bar transformation is chosen such that

$$\{\overline{\sigma}^\mu|\uparrow\uparrow\rangle\} \tag{21}$$

corresponds to an orthonormal basis of the local Hilbert space corresponding to one site and its auxiliary site. Therefore by the same generalization to multiple sites, the opEE of $U(t)$ will be identical to the wave function entanglement entropy of $|\psi(t)\rangle = \overline{U}(t)|\uparrow\cdots\uparrow\rangle$.

On the other hand, the bar transformation is an operator algebra isomorphism, which means for operators $O_1, O_2 \in \mathfrak{O}$, we have

$$\overline{O_1O_2} = \overline{O}_1\overline{O}_2. \tag{22}$$

For the time evolution operator of a time independent Hamiltonian (or each infinitesimal time evolution in the time ordered product), we have

$$\begin{aligned} \overline{e^{-iHt}} &= \overline{\lim_{n\to\infty}(1-iH\frac{t}{n})^n} \\ &= \lim_{n\to\infty}\overline{(1-iH\frac{t}{n})^n} = \lim_{n\to\infty}(1-i\overline{H}\frac{t}{n})^n \\ &= \exp(-i\overline{H}t). \end{aligned} \tag{23}$$

As a result, the opEE of $U(t)$ is equal to the state EE of $\exp(-i\overline{H}t)|\uparrow\cdots\uparrow\rangle$.

As argued above, the barred Hamiltonian will preserve the locality of interaction, (non-)integrability of the model and the spatial disorder distributions across the system. As a result, our knowledge of the global quench EE of those systems can be carried over.

We therefore expect that the opEE of the evolution operator will in general have three domains in its evolution with time. The behavior for times less than propagating over one lattice spacing should not be taken seriously, because of its regulator dependence. In the intermediate region when the EE is propagating through the system, the opEE will increase in a certain manner that is described by some scaling function (e.g. linear growth in CFT[32], power law in thermal phase[1,6], logarithmic growth in MBL phase[1–5,31]). In the thermal phase, the opEE will reach a saturation value which is extensive, however for integrable systems this may not be true due to the possible recurrence behavior[33].

B. The Page Value

Before analyzing the unitary time evolution of a physical Hamiltonian, let us first consider the average opEE of a random unitary operator, which will give us a guideline for the saturation behavior of random systems.

The average EE of a random wave function (with a measure that is invariant under unitary transformations, i.e. Haar measure) was derived by Page[34] to be

$$\begin{aligned} S_{\text{Page}} &= \left(\sum_{k=n+1}^{mn}\frac{1}{k}\right) - \frac{m-1}{2n} \\ &= \ln m - \frac{m}{2n} + \mathcal{O}(\frac{1}{mn}), \end{aligned} \tag{24}$$

where m and n are the dimensions of the Hilbert space of the two subsystems and $m \le n$.

To fix the notation for clarity, let us consider L sites hosted with $j = \frac{1}{2}$ spins in a chain with a bipartition in a smaller system (A) composed of ℓ_A spins (its complement B has then $\ell_B = L - \ell_A$ spins), then

$$S_{\text{Page}}[\psi] = \ell_A\ln 2 - 2^{\ell_A-\ell_B-1} + \mathcal{O}(2^{-L}). \tag{25}$$

For an equal partition ($\ell_A = \ell_B$)

$$S_{\text{Page}}[\psi] = \frac{L}{2}\ln 2 - \frac{1}{2} + \mathcal{O}(2^{-L}). \tag{26}$$

The deficit $\frac{1}{2}$ from the maximal possible EE here suggests a deviation from a maximally entangled state on average.

In App. B, we perform an analytic calculation based on an integration technique on the unitary group to show that the average opEE of a random unitary operator is indeed given by the Page value of a doubled system:

$$S_{\text{Page}}[\hat{U}] = 2\ell_A\ln 2 - 2^{2\ell_A-2\ell_B-1} + \mathcal{O}(4^{-L}). \tag{27}$$

The deficit for the even partition is again $\frac{1}{2}$.

In the analysis of our numerical results for the opEE of the evolution operator, we will compare the saturation values to the Page value.

IV. MODELS

We study various spin models to investigate the behavior of the opEE as a function of time. One of the simplest

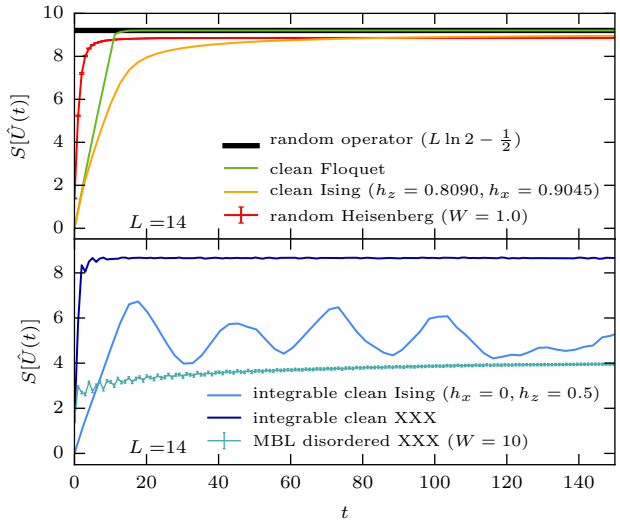


FIG. 2. Operator entanglement entropy $S[\hat{U}(t)]$ of the time evolution operator $\hat{U}(t)$ for the models introduced in Sec. IV as a function of time t. Top panel: Chaotic models. Bottom panel: Integrable (MBL) models. For all models, the opEE grows fast for short times and for the considered nonintegrable models, the opEE reaches a large value close to that of a random operator ($L \ln 2 - \frac{1}{2}$). For the clean integrable cases, the opEE fluctuates at large times due to commensurate periods of integrals of motion. The MBL model exhibits the slowest growth of the opEE with time. For the Floquet model, the opEE grows nearly linearly and saturates at the limit of a random unitary operator. The results for disordered models are averaged over 100 to 1000 realizations.

models is the Ising model in a tilted field

$$H = \sum_i \sigma_i^z \sigma_{i+1}^z + h_i^x \sigma_i^x + h_i^z \sigma_i^z, \tag{28}$$

with the Pauli matrix σ_i^μ on site i ($\mu = 1, 3$). Here, h_i^x (h_i^z) are the transverse (longitudinal) magnetic fields and we choose a homogeneous configuration without disorder. This model is integrable in the clean case if either h^x or h^z vanish, and non-integrable if both fields are non-zero with generic parameter choices. We adopt a popular set

$$h^x = 0.9045 \quad h^z = 0.8090 \tag{29}$$

to compare it with existing literature where it was argued that the system becomes robustly nonintegrable with these parameters[35–39].

We also study the *standard model* of MBL, the random field Heisenberg chain

$$H = \frac{1}{4} \sum_i \left[\sigma_i^x \sigma_{i+1}^x + \sigma_i^y \sigma_{i+1}^y + \sigma_i^z \sigma_{i+1}^z\right] + \frac{h_i^z}{2} \sigma_i^z \tag{30}$$

where h_i is the random field on site i. We take it to be drawn from a uniform distribution on the interval $[-W, W]$, where W is the disorder strength. This model has an MBL transition at a disorder strength of $W \approx 3.7$[14,40] and recent numerical evidence points to slow dynamics and subdiffusion at weaker disorder[1,41–45]. It conserves the total magnetization $S_z = \sum_i S_i^z$, and allows therefore to study only one magnetization sector. We project to the largest sector with $S_z = 0$, having a Hilbert space dimension of $\binom{L}{L/2}$. In the clean case $W = 0$, it is the integrable XXX chain.

While the Ising model in a tilted random field does not conserve magnetization, it still conserves energy. In order to have a completely generic quantum system, one can even break energy conservation by introducing periodic driving. We study a Floquet system with driving period τ given by the time evolution operator over one period

$$U(\tau) = \mathrm{e}^{-\mathrm{i}2H_{xy}\frac{\tau}{2}} \mathrm{e}^{-\mathrm{i}2H_z\frac{\tau}{2}} \tag{31}$$

where

$$\begin{aligned} H_{xy} &= \sum_i h_x^i \sigma_i^x + h_y^i \sigma_i^y, \quad h_x^i = 0.9045 \\ H_z &= \sum_i \sigma_i^z \sigma_{i+1}^z + h_z^i \sigma_i^z, \quad h_z^i = 0.8090 \end{aligned} \tag{32}$$

We set $\tau = 0.8$ and make two choices of h_y^i.

1. $h_y^i = 0$. This case has the same time averaged Hamiltonian as the chaotic Ising model evolution[37]. However the system is time-reversal invariant (by shifting half of the period, the unitary matrix is symmetric) and therefore corresponds to circular orthogonal ensemble (COE).

2. $h_y^i = 0.3457$. The σ^y term breaks the time reversal symmetry and thus $U(\tau)$ should be in the circular unitary ensemble (CUE).

Both choices lead to essentially identical behavior of the opEE, although in the CUE case, the dynamics seems to be slightly more chaotic, as we discuss in Fig. 6. With this exception, we study the COE model in the rest of this paper. We employ open boundary conditions throughout this work.

Fig. 2 gives an overview of the results for all these models with system size $L = 14$. In accordance with our state-quench mapping, the opEE has a fast growth at short times (except for the MBL case) and then saturates to a constant value for thermal phase, possibly oscillating in the integrable models. In the next few sections, we will address in detail the saturation value and the scaling of the growth respectively.

V. SATURATION VALUE

Let us first focus on the long time behavior of opEE $S[\hat{U}(t)]$ for various models. In nearly all systems that we considered, the opEE saturates to a constant value in Fig. 2 at sufficiently long times, and we classify them

as follows: Maximally scrambling behavior is found in the Floquet system, where $S[\hat{U}(t)]$ saturates to the Page value corresponding to a random unitary operator sampled from the Haar measure. Chaotic systems with conservation laws (energy, magnetization) also exhibit a large saturation value close to the Page value but with a small deficit which seems to be independent of system size and more conservation laws seem to lead to a larger deficit. In the MBL system with local integrals of motion the opEE saturates after a very long time at a value much smaller than the Page value, whereas clean integrable models with nonlocal conservation laws show no saturation of the opEE, but rather fluctuate more or less strongly around a value that is smaller than the Page value. From this observation, we speculate that the specific nature of the integrals of motion and presumably their incompatibility with the real space partition causes these fluctuations.

We will devote the rest of this section to the details of the two chaotic classes.

A. Floquet Spin Model

We study the Floquet spin model (31) introduced in Sec. IV as a typical model with no conservation laws. In previous studies, the average global quench EE of an initial product state after a long time evolution with the Floquet Hamiltonian was found to be given by the Page value $\frac{L}{2}\ln 2 - \frac{1}{2}$[36,37].

Fig. 2 illustrates that the numerically calculated opEE for the equal bipartition ($\ell_A = \ell_B$) saturates to $L\ln 2 - \frac{1}{2}$ in the long time limit. In App. B, we show that this is the average opEE of a random unitary operator by partly using Page's result for a random state[34]. This saturation value is in agreement with the consensus[46] that the Floquet evolution operator (without time reversal symmetry) is indeed a physical realization of the circular unitary ensemble.

In order to confirm this, we calculate the long time opEE $S[\hat{U}(\infty)]$ of the Floquet evolution operator for all possible bipartitions of the system and compare the results in Fig. 3 to

$$S_{\text{Page}} = 2\ell_A \ln 2 - 2^{2\ell_A - 2\ell_B - 1} \tag{33}$$

which is essentially the average opEE of a random unitary operator in the corresponding partition, where ℓ_A is the length of subsystem A and $\ell_B = (L - \ell_A)$ the correspondingly the length of its complement. The Floquet evolution operator opEE matches to the Page value for all possible partitions even in very small systems.

B. Chaotic systems with conservation laws

The next set of examples we consider in Fig. 2 are generically nonintegrable systems with conservation laws,

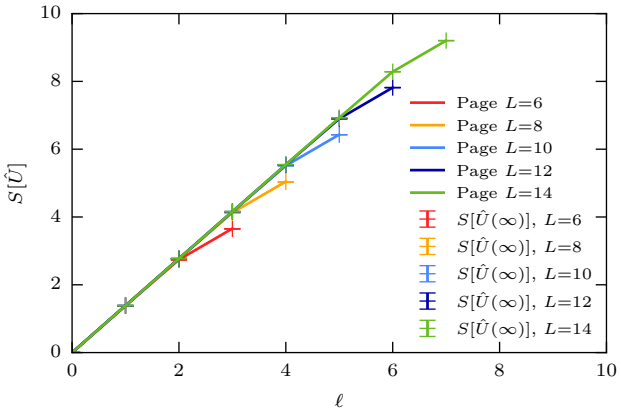


FIG. 3. Comparison of the saturation value of the opEE of the time evolution operator $S[\hat{U}(\infty)]$ (crosses, errorbars illustrate the size of fluctuations around the saturation value) of the Floquet model with the result for a random unitary operator (Page value, given by full lines) for all possible smaller subsystem sizes ℓ. The opEE for the Floquet system matches the Page result for all system sizes and partitions perfectly.

in particular the random field Heisenberg chain at weak disorder (such that it does not exhibit MBL[40]) and the tilted Ising chain. The former conserves energy and total magnetization, while the later was shown to be generically nonintegrable in Ref. 6 and conserves energy and parity under reflection.

We choose to present in detail the results of the Heisenberg model in a disordered field to show the different behaviors owing to the conservation laws and the locality of interactions.

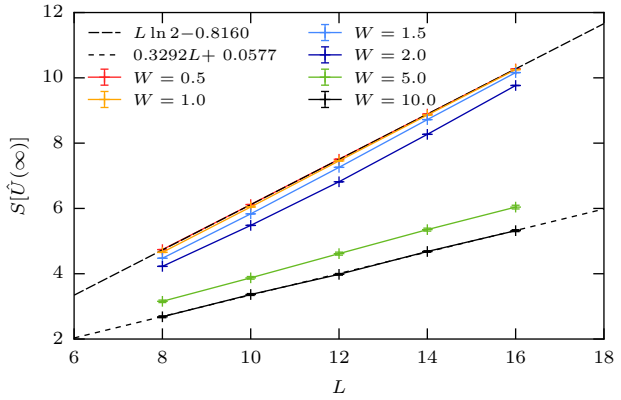


FIG. 4. Saturation value of the disorder averaged opEE for the equal bipartition for the random field Heisenberg model as a function of system size for different disorder strengths. For strong disorder $W \gtrsim 3.7$, the system is in the MBL phase and we observe a suppressed but extensive saturation value. At weak disorder, the saturation value scales as $L\ln 2$ but has a constant deficit.

The saturation behaviors for various disorder strengths

and different system sizes are shown in Fig. 4. For weak disorders, the saturation values is still around $L \ln 2$, but the deficit value is larger than $\frac{1}{2}$. When the disorder strength is so large that the system is in the MBL phase, the saturation value is extensive but is only a fraction of $L \ln 2$. Note that at weak disorder, there are visible finite size effects, as it seems that for larger system sizes, the saturation values for different disorder strengths approach each other. We suspect that for much larger system sizes, the deficit for disorder strengths below the MBL critical disorder becomes in fact equal, but will remain larger than $\frac{1}{2}$.

The MBL behavior is easy to be interpreted from the state-quench mapping discussed in Sec. III A. In fact, for systems deep inside MBL phase, the opEE can be directly mapped to the global quench of the *same* Hamiltonian, and so an upper bound for the saturation value is $\frac{L}{2} \ln 2$, which is indeed far less than the value in large chaotic systems.

In the next section, we ascribe the opEE deficit in the thermal phase to the block structure of the reduced density matrix, which ultimately is a result of the conserved total magnetization. We believe that a similar reasoning can also be applied to other thermal phase models with conservation laws, but an explicit demonstration is lacking.

C. Deficit Value of Random Field Heisenberg Model

The thermal phase saturation value of the chaotic models we studied is close to the maximal value, but the deficit is greater than that of the Floquet systems. Here we present an argument to explicitly show how the conservation law is responsible for this fact in a fixed magnetization sector ($S_z = 0$) of the Heisenberg model.

For simplicity, we will present this argument for the EE of a wave function and explain the generalization to the opEE in the end of this subsection.

The constraint $S_z = 0$ tells us that the S_z bases for part A and B have to be complementary, *i.e.* only states with $n_\uparrow$ up spins in A and $N - n_\uparrow$ up spins in B can be paired to form the basis of $S_z = 0$ sector of $2N$ sites (other combinations will yield a vanishing wave function coefficient).

Thus for any given state $|\psi\rangle$ with fixed magnetization $S_z = 0$, we can do a decomposition

$$|\psi\rangle = \sum_{n_\uparrow=0}^{N} \sum_{ij} \psi^{ij}_{n_\uparrow} |n_\uparrow, i\rangle_A |N - n_\uparrow, j\rangle_B \tag{34}$$

where $\psi^{ij}_{n_\uparrow}$ is a block matrix with $\binom{N}{n_\uparrow}$ rows and columns and ij are the row and column indices. This implies that the reduced density matrix is also block diagonal with size $\binom{N}{n_\uparrow}$ for each block. The operator version of this decomposition is just the one with a two-copy block size $\binom{N}{n_\uparrow}\binom{N}{n'_\uparrow}$. App. C gives a detailed account of how to utilize this structure in numerical computations.

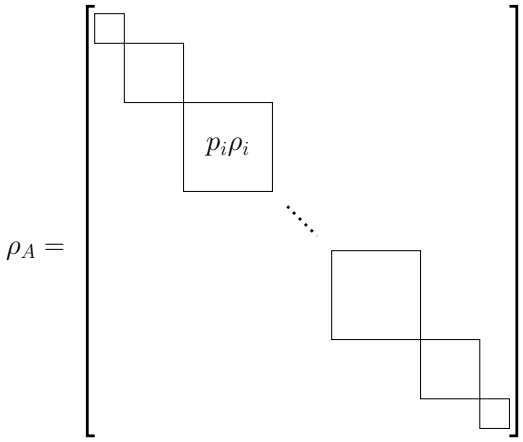


FIG. 5. Block diagonal form of the reduced density matrix.

Let the eigenvalues of the i-th block be $p^{(i)}_j$ (the index i is the same as $n_\uparrow$), and the trace of block i be $p_i = \sum_j p^{(i)}_j$, then the EE is

$$S = -\sum_{i,j} p^{(i)}_j \ln p^{(i)}_j = -\sum_i p_i \ln p_i - \sum_i p_i S_i, \tag{35}$$

where S_i is the EE of the i-th block

$$S_i = -\sum_j \frac{p^{(i)}_j}{p_i} \ln \frac{p^{(i)}_j}{p_i}. \tag{36}$$

If we regard each block rescaled by p_i to be a density matrix ρ_i, the total density matrix is then a classical mixture

$$\rho = \sum_i p_i \rho_i \qquad [\rho_i, \rho_j] = 0 \tag{37}$$

and the EE is the sum of the occupation entropy plus the average EE of all the blocks.

In principle, one should average the expression of S by a probability distribution of the occupation probability p_i and entropy distribution of S_i. For the sake of obtaining an upper bound, we can avoid this complication by just calculating the maximal value. The optimization problem

$$\max_{p_i} S[\{p_i\}] \quad \text{subject to} \quad \sum_i p_i = 1 \tag{38}$$

is easily solved by the Lagrangian multiplier technique and the maximal EE taking place at $p_i = \frac{e^{S_i}}{\sum_i e^{S_i}}$ is

$$S_{\max} = \ln \sum_i e^{S_i} \tag{39}$$

We estimate the upper bound by assuming that each ρ_i is a random block, and S_i takes the corresponding Page value of that block size. For the state, the block size is $\binom{N}{i}$ ($N = \frac{L}{2}$), and so

$$S_i \approx \ln \binom{N}{i} - \frac{1}{2}. \tag{40}$$

Although this is the not the exact result, only small i (in fact only $i = 0$ or N in the thermodynamic limit) will give an $\mathcal{O}(1)$ error which is negligible in the thermodynamic limit. As a result

$$S_{\max} = \ln \sum_i \binom{N}{i} - \frac{1}{2} = N \ln 2 - \frac{1}{2} \tag{41}$$

which is the Page value for state.

For the operators, the only thing that changes is that each block size becomes $\binom{N}{i}\binom{N}{j}$, and hence

$$S = \ln \sum_{ij} \binom{N}{i}\binom{N}{j} - \frac{1}{2} = 2N \ln 2 - \frac{1}{2} = L \ln 2 - \frac{1}{2}. \tag{42}$$

Since even the maximal value has a deficit $\frac{1}{2}$, we expect that in general after averaging over the distribution of p_i the average opEE is smaller and therefore has a larger deficit value.

VI. GROWTH

In the previous section, we studied the behavior of the opEE of the evolution operator at very long times in finite systems and found that a saturation value is reached. Since it is clear that at the initial time $t = 0$ the opEE is zero, we will now consider how the saturation value is reached in several example systems.

A. Growth of $S[\hat{U}(t)]$ for the Floquet model

In Fig. 6 we show the short time behavior of the opEE (equal bipartition) for the Floquet model (31) of different system sizes in both COE and CUE parameter choices. Clearly, the opEE grows very fast at short times and for different system sizes there are almost no visible finite size effects. We determine a fit to a power law growth at short times according to the form $S[\hat{U}(t)] = at^\alpha$ and obtain an exponent of $\alpha = 0.9641$ for COE system and $\alpha = 0.9967$ for CUE system. With the available system sizes it is difficult to determine whether the discrepancy in COE system from a perfect linear growth (which is for example observed in the growth of the quench EE in this model, starting from a product state[6]) is a finite size effect or prevails in the thermodynamic limit, but from the robustness of the result in Fig. 6, it is likely that the remaining time reversal symmetry leads to the deviation. After this initial almost ballistic growth, the opEE saturates to a value very close to the Page value as discussed in Sec. V A.

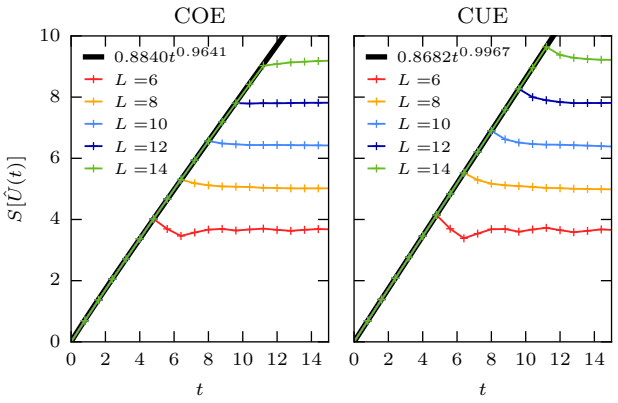


FIG. 6. Growth of the operator entanglement entropy in the Floquet model (31). The dashed lines correspond to a power law fit. Left panel: Floquet model with time reversal symmetry ($h_y^i = 0$), a small deviation from a linear growth is visible in the exponent. Right panel: Floquet model without time reversal symmetry ($h_y^i = 0.3457$), the linear growth is almost perfect.

These two results together are consistent with the expectation that the Floquet Hamiltonian can be considered as an almost perfect scrambler.

B. Growth of $S[\hat{U}(t)]$ in the random field Heisenberg chain

Let us now consider the growth of the opEE in the random field Heisenberg chain (30). We have already seen that the opEE at long times saturates to a value close to the Page limit, offset by a system size independent deficit, which we attributed to the constraints caused by conservation laws.

Here, we restrict ourselves to the case of weak disorder, where the Heisenberg chain is not fully many-body localized.

In Fig. 7, we show the growth of the disorder averaged opEE for different system sizes and disorder strengths. The saturation values obtained for very long times are displayed by dashed lines. It is obvious that the opEE of the evolution operator reaches the saturation value at much later times at stronger disorder ($W = 2$), compared to weak disorder ($W = 1$). This is consistent with the numerical evidence for slow dynamics in this region of the phase diagram, leading to a subballistic growth of the (state) entanglement entropy after a quench[1] and subdiffusive transport[1,15,41–44] (see Ref. 45 for a recent review of the numerical evidence).

To analyze the finite size scaling of the opEE of the evolution operator, we conjecture that the opEE will grow as a power law in time up to saturation, as was observed for the EE after a quench[1]. Then, we can make the scaling

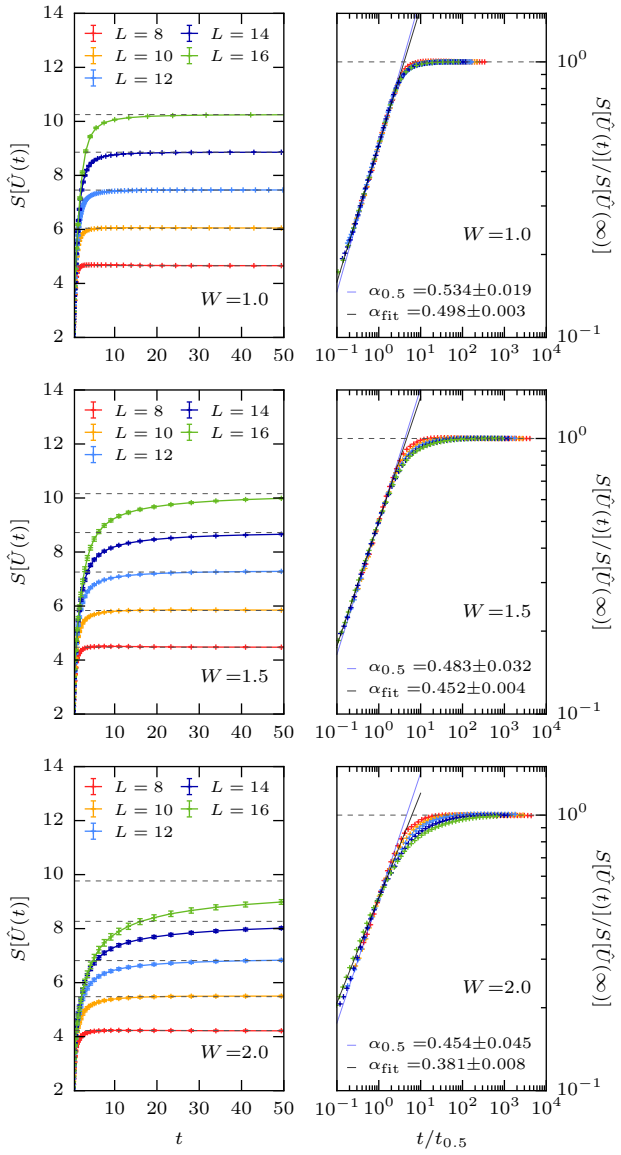


FIG. 7. (Left) Growth of the disorder averaged operator entanglement entropy of the evolution operator in the random field Heisenberg model ($S_z = 0$) at short times for various disorder strengths. (Right) Growth of the opEE in units of the saturation value S_∞ (dashed horizontal lines) as a function of time in units of the half saturation time $t_{0.5}$. We observe a power law growth at weak disorder with an exponent $\alpha < 1$, which is valid for intermediate times, when $t \approx t_{0.5}$. At stronger disorder, the exponent decreases and finite size effects are stronger, seemingly leading to a long domain of sup-power law growth of the opEE.

assumption that for hydrodynamic times (after an initial transient, but before the saturation), the opEE grows like $S[\hat{U}(t)] = \beta t^\alpha$ and thus we can estimate the time t_∞ after which the opEE saturates:

$$t_\infty \propto S(\infty)^{\frac{1}{\alpha}}, \tag{43}$$

where S_∞ is the saturation value $S[\hat{U}(\infty)]$

With this natural timescale in the problem, we propose the scaling hypothesis

$$S[\hat{U}(t)]/S(\infty) = f(t/t_\infty). \tag{44}$$

Numerically, it is difficult to determine the saturation time accurately, as in its proximity the power law growth seems to be violated. Therefore, we define instead the time $t_{0.5}$ at which the opEE reaches half of the saturation value by

$$S[\hat{U}(t_{0.5})] = \frac{S[\hat{U}(\infty)]}{2} \tag{45}$$

and use $t_{0.5}$ as the natural timescale. We determine this time by interpolating the time evolution of the opEE and solving Eq. (45) for $t_{0.5}$ numerically for each system size and disorder strength. The associated errorbar of $t_{0.5}$ is estimated by the error of the opEE divided by the derivative of the opEE with respect to time.

In the right panels of Fig. 7, we display the opEE divided by the saturation value $S[\hat{U}(\infty)]$ as a function of time in units of the half saturation time $t_{0.5}$ for different system sizes on a log-log scale. At weak disorder, all curves collapse almost perfectly to one universal curve, displaying a clear power law for $t \sim t_{0.5}$. For stronger disorder, finite size effects become more visible but it seems that the curves still converge to a universal curve for larger system sizes. At a disorder strength of $W = 2$ (bottom panel), the power law regime is shorter than at weaker disorder and at intermediate times an extended regime of slow growth of the opEE is visible in the curvature of the curve. Currently, it is unclear where this regime comes from, but we may speculate that it is due to the fact that at this disorder strength for finite systems a fraction of the eigenstates of the Hamiltonian are already many-body localized[40]. Although there is no direct connection to the behavior of the eigenstates of the Hamiltonian, to the growth of the opEE of the evolution operator can be influenced by this fact and therefore exhibit slower dynamics. At weaker disorder, the fraction of localized states in the spectrum of the Hamiltonian is much smaller and therefore the effect of slower dynamics can be expected to be less visible, which is the case in our results.

Let us finally address the power law growth of the opEE at short times. In the previous subsection, we have shown that for a Floquet system, the growth is almost linear, however in the random Heisenberg chain slower dynamics can be expected. We use two methods to determine the exponent of the power law growth: First, we fit a power law to the growth of the opEE in time for the largest system size over a time window where it appears to be linear on a log-log scale, yielding an exponent $\alpha_{\rm fit}$. The fit and the value of the exponent is reported in Fig. 7. The second approach relies on the scaling ansatz, since according to the scaling arguments explained above, we expect that

$$t_{0.5} \propto L^{\frac{1}{\alpha}}, \tag{46}$$

and we can use this ansatz to fit a power law to $t_{0.5}(L)$, yielding $\alpha_{0.5}$. Both exponents agree reasonably well with errorbars. We also show the corresponding power law curves together with the data collapse for comparison.

C. Growth of $S[\hat{U}(t)]$ in the MBL phase

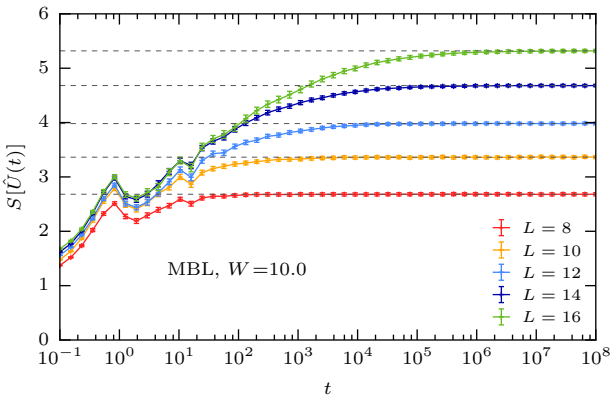


FIG. 8. Growth of the operator entanglement entropy in the MBL phase of the random Heisenberg model ($S_z = 0$).

It is known that the entanglement dynamics in MBL systems is much slower than in ergodic systems, in fact after a quench, the (state) entanglement entropy grows logarithmically and saturates to a volume law value with a suppressed prefactor[1,3,4,31].

In Fig. 8, we show the disorder averaged opEE of the evolution operator for different system sizes of the random field Heisenberg chain (30) at strong disorder $W = 10$, where the system is surely in the MBL phase. On a logarithmic scale in time, it is visible that the saturation value is approached extremely slowly and our results are consistent with a logarithmic growth of the opEE, although larger system sizes would be required to test this hypothesis thoroughly.

VII. CONCLUSION

We have defined the opEE of the time evolution operator and analyzed the saturation and growth patterns in various spin systems.

The Floquet system is the most chaotic among the models we studied. It has a linear initial growth of the opEE saturating at the Page value: the average EE of a random unitary operator. We also consider another chaotic system with global conservation laws: the Heisenberg model with disorder field. There, we find a power law growth with an almost perfect data collapse in the weak disorder regime and a saturation value only less than the Page value by an non-extensive amount. We believe that the conservation law and locality of the interaction is responsible for the slower growth and smaller saturation value (compared to Floquet model). The opEE in the MBL phase exhibits a logarithmic growth in time and saturates to an extensive value which is given by a fraction of the saturation value in chaotic models.

Due to the quench mapping in Sec. III A, we understand the behavior of opEE through the knowledge of the wave function EE after a global quench. Yet one advantage of the opEE is its initial state independence. It is therefore useful to characterize the scrambling properties of the time evolution operator itself.

The the channel-state duality in App. A gives us a double-system picture that also emerges in the thermofield double state in the study of the holography with the presence of the eternal black hole[47]. The opEE is the state EE of the global quenched dual state, and in the gravity dual, the Ryu-Takayanagi surface[48] will probe behind the horizon of the black hole[49]. It would be interesting to reproduce the scaling and saturation in a holographic calculation.

ACKNOWLEDGMENTS

TZ benefited from discussions with Mark K. Mezei and Thomas Faulkner about the holographic interpretation of the quench EE. TZ is supported by the National Science Foundation under grant number NSF-DMR-1306011. DJL is grateful for discussions with Yevgeny Bar Lev. We are appreciate Tomaž Prosen's effort of reading the manuscript and providing comments on the distinction of COE and CUE and thank Fabien Alet and Yevgeny Bar Lev for their comments on the manuscript. This work was supported in part by the Gordon and Betty Moore Foundation's EPiQS Initiative through Grant No. GBMF4305 at the University of Illinois. This work made use of the Illinois Campus Cluster, a computing resource that is operated by the Illinois Campus Cluster Program (ICCP) in conjunction with the National Center for Supercomputing Applications (NCSA) and which is supported by funds from the University of Illinois at Urbana-Champaign.

Appendix A: Channel-State Duality

Here we view the opEE in the light of the channel-state duality originated from the quantum information community. We restrict to the unitary channel that is relevant to the opEE. A more detailed account and application can be found for example in Ref. 50 and 51.

For any linear operator expanded in a basis $|i\rangle \in \mathcal{H}$,

$$U = \sum_{ij} U_{ij} |i\rangle\langle j| \tag{A1}$$

we can always construct a corresponding state $|\psi\rangle$ in the enlarged Hilbert space $\mathcal{H} \times \mathcal{H}$

$$|\psi\rangle = \sum_{ij} |i\rangle \otimes U_{ij} |j\rangle^* = \sum_{i} |i\rangle \otimes U |i\rangle^*. \tag{A2}$$

Operationally, we just replace the bra $\langle j|$ by a ket $|j\rangle^*$ which is the complex conjugation of the state $|j\rangle$. This choice makes the state $|\psi\rangle$ basis independent, which can be easily verified by doing another unitary transformation V

$$\begin{aligned} |\psi'\rangle &= \sum_{i'} |i'\rangle \otimes U |i'\rangle^* = \sum_{i'ij} V_{i'i} V^*_{i'j} |i\rangle \otimes U |j\rangle^* \\ &= \sum_{ij} \delta_{ij} |i\rangle \otimes U |j\rangle^* = |\psi\rangle. \end{aligned} \tag{A3}$$

So this unique state $|\psi\rangle$ dual to the unitary operator U contains all its information, and one can study this state instead to gain knowledge of the operator.

The dual state is defined on two copies of the original system, and the unitary operator is acting only on one of them. Partitioning of the operator corresponds to an identical space partitions in these two copies of system, which is shown in Fig. 9. The opEE is the then identical to the state EE of the A, B partition for the dual state $|\psi\rangle$. We

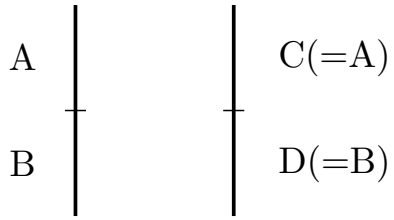


FIG. 9. Channel state duality point of view of opEE. The vertical lines correspond to the two copies of the original system and the bipartition of the system into A and B has to be performed equally in both copies.

use this picture for computing analytically the average opEE of a random unitary operator in App. B.

Appendix B: Average opEE of Random Unitary Operator

In this appendix, we prove that the average opEE of random unitary operator (circular unitary ensemble) is equal to the Page value.

We use the standard replica trick and average over the Haar measure $[dU]$ of the unitary group $\mathrm{U}(N)$ to compute the EE

$$\bar{S}[U] = -\int [dU]\, \partial_n \mathrm{Tr}(\rho^n[U])\Big|_{n=1} \tag{B1}$$

and further assume that the derivative and integral commute, so that we can compute the average first

$$\overline{\mathrm{Tr}(\rho^n)} = \int [dU]\, \mathrm{Tr}(\rho^n[U]) \tag{B2}$$

In a chosen basis, the matrix element can be written as $U_{i_A j_B, \bar{i}_A \bar{j}_B}$, where the combination of i_A, j_B exhausts the indices for a state (left line of Fig. 9), and the same for $\bar{i}_A$, $\bar{j}_B$ (right line of Fig. 9). We need a partial transpose to obtain the expansion coefficient in the operator basis

$$U_{i_A j_B, \bar{i}_A \bar{j}_B} \to U_{i_A \bar{i}_A, j_B \bar{j}_B} \tag{B3}$$

where now i_A and $\bar{i}_A$ are indexing the A_i basis etc. The density matrix for the operator is then

$$\rho[U]_{i_A \bar{i}_A, i'_A \bar{i}'_A} = U_{i_A \bar{i}_A, j_B \bar{j}_B} U^*_{j_B \bar{j}_B, i'_A \bar{i}'_A}, \tag{B4}$$

summing over repeated indices. The diagrammatic representation in Fig. 10 can guide[51] us to write down the complicated index structure of $\mathrm{Tr}(\rho^n[U])$. For a $2^n \times 2^n$ matrix $U_{i_A j_B, \bar{i}_A \bar{j}_B}$, the upper two closed lines on each block

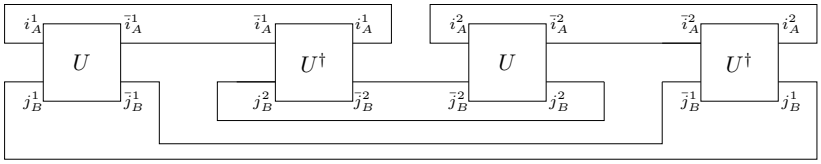


FIG. 10. Diagrammatic representation of $\mathrm{Tr}(\rho^2[U])$.

represents A region indices $i_A, \bar{i}_A$ and the lower two closed lines represents B region indices $j_B, \bar{j}_B$. The two ends of connecting lines are contracting indices. So for example, the diagram in Fig. 10 can be translated to

$$\begin{aligned}\mathrm{Tr}(\rho^2[U]) =& U_{i_A^1 j_B^1, \bar{i}_A^1 \bar{j}_B^1} \left(U^\dagger\right)_{\bar{i}_A^1 \bar{j}_B^2, i_A^1 j_B^2} U_{i_A^2 j_B^2, \bar{i}_A^2 \bar{j}_B^2} \left(U^\dagger\right)_{\bar{i}_A^2 \bar{j}_B^1, i_A^2 j_B^1} \\ =& U_{i_A^1 j_B^1, \bar{i}_A^1 \bar{j}_B^1} U^*_{i_A^1 j_B^2, \bar{i}_A^1 \bar{j}_B^2} U_{i_A^2 j_B^2, \bar{i}_A^2 \bar{j}_B^2} U^*_{i_A^2 j_B^1, \bar{i}_A^2 \bar{j}_B^1}\end{aligned} \tag{B5}$$

where $*$ represents the complex conjugate the indexed element.

The same type of integral also appears in the discussion of Haar scrambling in Ref. 52 and 51, where the $n = 2$ case is calculated by the Weingarten formula to obtain the Rényi entropy. We here apply the general Weingarten formula for the integration on the unitary group,

$$\begin{aligned}&\int [dU] U_{i_1, j_1} U_{i_2, j_2} \dots U_{i_n, j_n} U^*_{i'_1, j'_1} U^*_{i'_2, j'_2} \dots U^*_{i'_n, j'_n} \\ &\quad = \sum_{\sigma, \tau \in S_n} \delta_{i_1 i'_{\sigma(1)}} \delta_{i_2 i'_{\sigma(2)}} \dots \delta_{i_n i'_{\sigma(n)}} \delta_{j_1 j'_{\tau(1)}} \delta_{j_2 j'_{\tau(2)}} \dots \delta_{j_n j'_{\tau(n)}} \mathrm{Wg}(N, \sigma\tau^{-1})\end{aligned} \tag{B6}$$

where the sum is taken over all possible permutations in S_n, and N is the size of the matrix 2^L. Wg is the Weingarten function (see detailed definition and the first few examples in Ref. 53), whose large N limit (thermodynamic limit)[53] is given by

$$\mathrm{Wg}(N, \sigma) = \frac{1}{N^{n+|\sigma|}} \Big[\prod_{\sigma = C_1 C_2 \cdots C_k} (-1)^{|C_i|-1} \mathrm{Catalan}_{|C_i|} + \mathcal{O}(N^{-2}) \Big] \tag{B7}$$

where the C_i are the cycle decomposition of σ , $|C_i|$ are the number of elements in this cycle, Catalan is the Catalan number, $|\sigma|$ is its Cayley distance to the identity (minimal number of transpositions that makes it identity). Obviously, the dominant term in $N \to \infty$ limit is the one with $\sigma = e$

$$\mathrm{Wg}(N, e) = \frac{1}{N^n} + \mathcal{O}(N^{-n-2}) \tag{B8}$$

In the integration of the U it means that only $\sigma = \tau$ are relevant, i.e. the i index and j index share the same permutation

$$\int [dU] \cdots \sim \frac{1}{N^n} \sum_{\sigma \in S_n} \delta_{i_1 i'_{\sigma(1)}} \delta_{i_2 i'_{\sigma(2)}} \dots \delta_{i_n i'_{\sigma(n)}} \delta_{j_1 j'_{\sigma(1)}} \delta_{j_2 j'_{\sigma(2)}} \dots \delta_{j_n j'_{\sigma(n)}} \tag{B9}$$

The contractions of these delta function can be converted to loop counting in planar diagrams. Let us illustrate the example of $n = 2$

$$\int [dU] \mathrm{Tr}(\rho^2[U]) = \int [dU]\, U_{i_A^1 j_B^1, \bar{i}_A^1 \bar{j}_B^1} U^*_{i_A^1 j_B^2, \bar{i}_A^1 \bar{j}_B^2} U_{i_A^2 j_B^2, \bar{i}_A^2 \bar{j}_B^2} U^*_{i_A^2 j_B^1, \bar{i}_A^2 \bar{j}_B^1} \tag{B10}$$



FIG. 11. Eight indices in $\mathrm{Tr}(\rho^2[U])$, where contractions are performed for the 4 pairs.

where the four indices may be represented as the lids in Fig. 11 After doing the integration, the delta functions for each permutation element σ will close these diagrams. For example when $\sigma = (12)$, there are 1×2 loops for A indices and 2×2 loops for B indices, and then the corresponding factor is $2^{2\ell_A + 4\ell_B}$.



FIG. 12. Delta functions for each permutation element σ will close these diagrams. Each loop will contribute a $(2^{\ell_A})^2$ or (2^{ℓ_B}), where the square is for two copies of indices.

The loop counting is a combinatorial problem that can be formulated as solving the following generating function (by trial and error). Let

$$f_n(x, y) = \sum_{g \in S_n} x^{\chi(g)} y^{\chi(\tau g)} \tag{B11}$$

where $\chi(g)$ is the number of cycles in the permutation and $\tau = (12 \cdots n)$. The average of the trace can be expressed by this polynomial

$$\overline{\mathrm{Tr}(\rho^n[U])} = \frac{1}{(2^{2\ell_A + 2\ell_B})^n} f_n(4^{\ell_A}, 4^{\ell_B}) = \frac{1}{4^{nL}} f_n(4^{\ell_A}, 4^{\ell_B}) \tag{B12}$$

At this point, we can apply Page's state result as a shortcut. For a random state, the component of the wavefunction is

$$\psi_{\bar{i}_A \bar{j}_B} = U_{1, \bar{i}_A \bar{j}_B} \tag{B13}$$

where U is again taken from the Haar measure. Then the state version of integral for $n = 2$ is

$$\int [dU] \mathrm{Tr}(\rho^2[\psi]) = \int [dU]\, U_{1, \bar{i}_A^1 \bar{j}_B^1} U^*_{1, \bar{i}_A^1 \bar{j}_B^2} U_{1, \bar{i}_A^2 \bar{j}_B^2} U^*_{1, \bar{i}_A^1 \bar{j}_B^1} \tag{B14}$$

The whole process using the Weingarten formula and its asymptotics can be similarly applied; the only difference is that the state only has the barred set of indices

$$\overline{\mathrm{Tr}(\rho^n[\psi])} = \frac{1}{2^{nL}} f_n(2^{\ell_A}, 2^{\ell_B}) \tag{B15}$$

so the opEE will be the Page value of a state with length $2L$ and partition $2\ell_A + 2\ell_B = 2L$, *i.e.*

$$S[U] = 2\ell_A \ln 2 - 2^{2\ell_A - 2\ell_B - 1} \tag{B16}$$

We also manage to do a direct combinatorial computation for equal partition, where the top coefficient of the generating function[54] a_n (cf. Ref. 55 for why the top power is $n+1$ and the concept of genus)

$$f_n(x, x) = \sum_{g \in S_n} x^{\chi(g) + \chi(\tau g)} = a_n x^{n+1} + \cdots \tag{B17}$$

determines the trace

$$\overline{\mathrm{Tr}(\rho^n[\psi])} = \frac{1}{4^{nL}} f_n(4^{\frac{L}{2}}, 4^{\frac{L}{2}}) = \frac{a_n}{2^{(n-1)L}} + \mathcal{O}(\frac{1}{2^{nL}}). \tag{B18}$$

By analytic continuation, the EE is

$$S[U] = L \ln 2 - \partial_n a_n \Big|_{n=1} + \mathcal{O}(\frac{1}{2^L}). \tag{B19}$$

Through a series of bijections, a_n can be proven to be equal to the Catalan number(exercise 118 of Refs. 54, 56)

$$a_n = \frac{2n!}{n!(n+1)!} \tag{B20}$$

Therefore

$$\partial_n \frac{2n!}{n!(n+1)!}\Big|_{n=1} = \partial_n \frac{1}{n(n+1)B(n,n+1)}\Big|_{n=1} = \frac{1}{2} \tag{B21}$$

gives us the correct deficit of the Page value

$$S = L\ln 2 - \frac{1}{2} \tag{B22}$$

Appendix C: Lin Table Algorithm for $S_z = 0$ Sector

We take the σ_z basis in the Hilbert space, each of which are eigenvectors of total $\sum_i \sigma_i^z$. Consider the subspace where the eigenvalue of the total S^z is zero. Each basis state then has an equal number of $\uparrow$ spins and $\downarrow$ spins. In a $2N$ sites system, the dimension of the subspace is $\binom{2N}{N}$.

For any state in this subspace, we can take advantage of the constraint to do a partial Schmidt decomposition

$$|\psi\rangle = \sum_{n_\uparrow} \sum_{ij} \psi^{ij}_{n_\uparrow} |n_\uparrow, i\rangle_A |n - n_\uparrow, j\rangle_B \tag{C1}$$

where $\psi^{ij}_{n_\uparrow}$ is a block diagonal matrix, the number of up spins $n_\uparrow$ in part A is the block index and ij are the row and column indices within the block. The dimension of each block is $\binom{N}{n_\uparrow}^2$, and the identity

$$\sum_{n_\uparrow=0}^{N} \binom{N}{n_\uparrow}^2 = \binom{2N}{N} \tag{C2}$$

ensure that the coefficients from the σ^z basis wavefunction to the block elements $\psi^{ij}_{n_\uparrow}$ is just a permutation.

We use a 2N-bit binary number to represent the σ^z basis. In the example of $N = 3$, the σ^z basis wavefunction wavefunction elements are

	000	001	010	011	100	101	110	111
000								ψ_1
001				ψ_2		ψ_3	ψ_4	
010				ψ_5		ψ_6	ψ_7	
011		ψ_8	ψ_9		ψ_{10}			
100				ψ_{11}		ψ_{12}	ψ_{13}	
101		ψ_{14}	ψ_{15}		ψ_{16}			
110		ψ_{17}	ψ_{18}		ψ_{19}			
111	ψ_{20}							

(C3)

and the corresponding $\psi^{ij}_{n_\uparrow}$ matrix is

	111	(011	101	110)	(001	010	100)	000
000	ψ_1							
001		ψ_2	ψ_3	ψ_4				
010		ψ_5	ψ_6	ψ_7				
100		ψ_{11}	ψ_{12}	ψ_{13}				
011					ψ_8	ψ_9	ψ_{10}	
101					ψ_{14}	ψ_{15}	ψ_{16}	
110					ψ_{17}	ψ_{18}	ψ_{19}	
111								ψ_{20}

(C4)

If we store $\psi^{ij}_{n\uparrow}$ in a row vector, then the index of ψ will be

$$(1, 2, 3, 4, 5, 6, 7, 11, 12, 13, 8, 9, 10, 14, 15, 16, 17, 18, 19, 20) \tag{C5}$$

The permutation element we are looking for in this $n = 3$ example is $(8, 11), (9, 12), (10, 13)$. The algorithm needs to figure out the conversion table from the σ^z basis elements to the block elements and then do the Schmidt decomposition for each blocks, which is much more efficient than doing it in the full Hilbert space. We note that this can be done efficiently using the method of Lin tables as pointed out by H. Lin in Ref. 57.

* tzhou13@illinois.edu

[1] David J. Luitz, Nicolas Laflorencie, and Fabien Alet, "Extended slow dynamical regime close to the many-body localization transition," Phys. Rev. B **93**, 060201 (2016).

[2] Gabriele De Chiara, Simone Montangero, Pasquale Calabrese, and Rosario Fazio, "Entanglement entropy dynamics of Heisenberg chains," J. Stat. Mech. **2006**, P03001 (2006).

[3] Marko Žnidarič, Tomaž Prosen, and Peter Prelovšek, "Many-body localization in the Heisenberg XXZ magnet in a random field," Phys. Rev. B **77**, 064426 (2008).

[4] Jens H. Bardarson, Frank Pollmann, and Joel E. Moore, "Unbounded Growth of Entanglement in Models of Many-Body Localization," Phys. Rev. Lett. **109**, 017202 (2012).

[5] Maksym Serbyn, Z. Papić, and Dmitry A. Abanin, "Universal Slow Growth of Entanglement in Interacting Strongly Disordered Systems," Physical Review Letters **110**, 260601 (2013).

[6] Hyungwon Kim and David A. Huse, "Ballistic Spreading of Entanglement in a Diffusive Nonintegrable System," Phys. Rev. Lett. **111**, 127205 (2013).

[7] Bela Bauer and Chetan Nayak, "Area laws in a many-body localized state and its implications for topological order," J. Stat. Mech. **2013**, P09005 (2013).

[8] Jonas A. Kjäll, Jens H. Bardarson, and Frank Pollmann, "Many-Body Localization in a Disordered Quantum Ising Chain," Phys. Rev. Lett. **113**, 107204 (2014).

[9] Ronen Vosk, David A. Huse, and Ehud Altman, "Theory of the Many-Body Localization Transition in One-Dimensional Systems," Phys. Rev. X **5**, 031032 (2015).

[10] Andrew C. Potter, Romain Vasseur, and S. A. Parameswaran, "Universal Properties of Many-Body Delocalization Transitions," Phys. Rev. X **5**, 031033 (2015).

[11] Xiao Chen, Xiongjie Yu, Gil Young Cho, Bryan K. Clark, and Eduardo Fradkin, "Many-body localization transition in Rokhsar-Kivelson-type wave functions," Phys. Rev. B **92**, 214204 (2015).

[12] David J. Luitz, "Long tail distributions near the many body localization transition," Physical Review B **93** (2016), 10.1103/PhysRevB.93.134201, arXiv: 1601.04058.

[13] Xiongjie Yu, David J. Luitz, and Bryan K. Clark, "Bimodal entanglement entropy distribution in the many-body localization transition," Physical Review B **94** (2016), 10.1103/PhysRevB.94.184202, arXiv: 1606.01260.

[14] Arijeet Pal and David A. Huse, "Many-body localization phase transition," Phys. Rev. B **82**, 174411 (2010).

[15] David J. Luitz and Yevgeny Bar Lev, "Anomalous thermalization in ergodic systems," Physical Review Letters **117** (2016), 10.1103/PhysRevLett.117.170404, arXiv: 1607.01012.

[16] J. M. Deutsch, "Quantum statistical mechanics in a closed system," Phys. Rev. A **43**, 2046–2049 (1991).

[17] Mark Srednicki, "Chaos and quantum thermalization," Phys. Rev. E **50**, 888–901 (1994).

[18] Marcos Rigol, Vanja Dunjko, and Maxim Olshanii, "Thermalization and its mechanism for generic isolated quantum systems," Nature **452**, 854–858 (2008).

[19] Tomaž Prosen and Iztok Pižorn, "Operator space entanglement entropy in a transverse Ising chain," Phys. Rev. A **76**, 032316 (2007).

[20] Iztok Pižorn and Tomaž Prosen, "Operator space entanglement entropy in XY spin chains," Physical Review B **79**, 184416 (2009).

[21] Tomaž Prosen, "Chaos and complexity of quantum motion," Journal of Physics A: Mathematical and Theoretical **40**, 7881 (2007).

[22] Ulrich Schollwoeck, "The density-matrix renormalization group in the age of matrix product states," Annals of Physics **326**, 96–192 (2011), arXiv: 1008.3477.

[23] David Pekker and Bryan K. Clark, "Encoding the structure of many-body localization with matrix product operators," arXiv:1410.2224 [cond-mat] (2014), arXiv: 1410.2224.

[24] Frank Pollmann, Vedika Khemani, J. Ignacio Cirac, and S. L. Sondhi, "Efficient variational diagonalization of fully many-body localized Hamiltonians," Phys. Rev. B **94**, 041116 (2016).

[25] Maksym Serbyn, Z. Papić, and Dmitry A. Abanin, "Local Conservation Laws and the Structure of the Many-Body Localized States," Phys. Rev. Lett. **111**, 127201 (2013).

[26] David A. Huse, Rahul Nandkishore, and Vadim Oganesyan, "Phenomenology of fully many-body-localized systems," Phys. Rev. B **90**, 174202 (2014).

[27] Rahul Nandkishore and David A. Huse, "Many-Body Localization and Thermalization in Quantum Statistical Mechanics," Annu. Rev. Condens. Matter Phys. **6**, 15–38 (2015).

[28] John Z. Imbrie, "On Many-Body Localization for Quantum Spin Chains," J Stat Phys **163**, 998–1048 (2016).
[29] John Z. Imbrie, "Diagonalization and Many-Body Localization for a Disordered Quantum Spin Chain," Phys. Rev. Lett. **117**, 027201 (2016).
[30] J. Z. Imbrie, V. Ros, and A. Scardicchio, "Review: Local Integrals of Motion in Many-Body Localized systems," arXiv:1609.08076 [cond-mat, physics:math-ph] (2016), arXiv: 1609.08076.
[31] Rajeev Singh, Jens H. Bardarson, and Frank Pollmann, "Signatures of the many-body localization transition in the dynamics of entanglement and bipartite fluctuations," New J. Phys. **18**, 023046 (2016).
[32] Pasquale Calabrese and John Cardy, "Evolution of Entanglement Entropy in One-Dimensional Systems," Journal of Statistical Mechanics: Theory and Experiment **2005**, P04010 (2005), arXiv: cond-mat/0503393.
[33] John Cardy, "Quantum Revivals in Conformal Field Theories in Higher Dimensions," arXiv:1603.08267 [cond-mat, physics:hep-th] (2016), arXiv: 1603.08267.
[34] Don N. Page, "Average entropy of a subsystem," Physical Review Letters **71**, 1291–1294 (1993).
[35] Tomaž Prosen, "General relation between quantum ergodicity and fidelity of quantum dynamics," Physical Review E **65** (2002), 10.1103/PhysRevE.65.036208.
[36] Liangsheng Zhang, Hyungwon Kim, and David A. Huse, "Thermalization of entanglement," arXiv:1501.01315 [cond-mat, physics:quant-ph] (2015), arXiv: 1501.01315.
[37] Liangsheng Zhang, Vedika Khemani, and David A. Huse, "A Floquet Model for the Many-Body Localization Transition," arXiv:1609.00390 [cond-mat] (2016), arXiv: 1609.00390.
[38] M. Akila, D. Waltner, B. Gutkin, and T. Guhr, "Particle-Time Duality in the Kicked Ising Chain I: The Dual Operator," Journal of Physics A: Mathematical and Theoretical **49**, 375101 (2016), arXiv: 1602.07130.
[39] M. Akila, D. Waltner, B. Gutkin, and T. Guhr, "Particle-Time Duality in the Kicked Ising Chain II: Applications to the Spectrum," arXiv:1602.07479 [cond-mat, physics:nlin, physics:quant-ph] (2016), arXiv: 1602.07479.
[40] David J. Luitz, Nicolas Laflorencie, and Fabien Alet, "Many-body localization edge in the random-field Heisenberg chain," Physical Review B **91** (2015), 10.1103/PhysRevB.91.081103, arXiv: 1411.0660.
[41] Yevgeny Bar Lev and David R. Reichman, "Dynamics of many-body localization," Phys. Rev. B **89**, 220201 (2014).
[42] Yevgeny Bar Lev, Guy Cohen, and David R. Reichman, "Absence of Diffusion in an Interacting System of Spinless Fermions on a One-Dimensional Disordered Lattice," Phys. Rev. Lett. **114**, 100601 (2015).
[43] Kartiek Agarwal, Sarang Gopalakrishnan, Michael Knap, Markus Müller, and Eugene Demler, "Anomalous Diffusion and Griffiths Effects Near the Many-Body Localization Transition," Phys. Rev. Lett. **114**, 160401 (2015).
[44] Marko Žnidarič, Antonello Scardicchio, and Vipin Kerala Varma, "Diffusive and Subdiffusive Spin Transport in the Ergodic Phase of a Many-Body Localizable System," Phys. Rev. Lett. **117**, 040601 (2016).
[45] David J. Luitz and Yevgeny Bar Lev, "The Ergodic Side of the Many-Body Localization Transition," arXiv:1610.08993 [cond-mat] (2016), arXiv: 1610.08993.
[46] Fritz Haake, *Quantum Signatures of Chaos*, Springer Series in Synergetics, Vol. 54 (Springer Berlin Heidelberg, Berlin, Heidelberg, 2010).
[47] Juan M. Maldacena, "Eternal Black Holes in AdS," Journal of High Energy Physics **2003**, 021–021 (2003), arXiv: hep-th/0106112.
[48] Shinsei Ryu and Tadashi Takayanagi, "Aspects of holographic entanglement entropy," Journal of High Energy Physics **2006**, 045 (2006).
[49] Thomas Hartman and Juan Maldacena, "Time evolution of entanglement entropy from black hole interiors," arXiv preprint arXiv:1303.1080 (2013).
[50] Min Jiang, Shunlong Luo, and Shuangshuang Fu, "Channel-state duality," Physical Review A **87**, 022310 (2013).
[51] Pavan Hosur, Xiao-Liang Qi, Daniel A. Roberts, and Beni Yoshida, "Chaos in quantum channels," Journal of High Energy Physics **2016**, 1–49 (2016).
[52] Stephen H. Shenker and Douglas Stanford, "Black holes and the butterfly effect," Journal of High Energy Physics **2014**, 67 (2014).
[53] Benoît Collins and Piotr Śniady, "Integration with Respect to the Haar Measure on Unitary, Orthogonal and Symplectic Group," Communications in Mathematical Physics **264**, 773–795 (2006).
[54] Richard P. Stanley, *Catalan Numbers* (Cambridge University Press, Cambridge, 2015).
[55] Serge Dulucq and Rodica Simion, "Combinatorial Statistics on Alternating Permutations," Journal of Algebraic Combinatorics **8**, 169–191.
[56] Rodica Simion, "Noncrossing partitions," Discrete Mathematics **217**, 367–409 (2000).
[57] H. Q. Lin, "Exact diagonalization of quantum-spin models," Phys. Rev. B **42**, 6561–6567 (1990).